Hindawi
Journal of Advanced Transportation
Volume 2022, Article ID 8445650, 7 pages
https://doi.org/10.1155/2022/8445650

Research Article

Analysis of Fuel Tank Collision Structure Based on Defense Point Method

Wenguang Liu,[1,2] **Haijiang Liu**,[2] **Lin Jiang**,[3] **and Shanshan Bi**[1]

[1]*School of Automotive and Traffic Engineering, Jiangsu University, 301 Xuefu Road, Zhenjiang, Jiangsu, China*
[2]*Tongji University, Shanghai, China*
[3]*YAPP Automotive Systems Co., Ltd., Yangzhou, China*

Correspondence should be addressed to Wenguang Liu; liuwg@ujs.edu.cn

Received 6 April 2022; Revised 17 May 2022; Accepted 21 June 2022; Published 10 August 2022

Academic Editor: Sang-Bing Tsai

Aiming at the impact process of a fuel tank, which is a transient energy conversion process, the material absorbs energy through deformation to analyze the mechanical properties of the fuel tank during the impact process. The defense node method is adopted to simulate the dynamic response of the fuel tank during impact. The results show that it can accurately evaluate the safety of the container.

1. Introduction

The automobile fuel tank is the important component of the automobile fuel supply system. The country has strict requirements for its safety and environmental protection. To make full use of the limited automotive chassis space and adapt to various vehicle types, the shape of the automobile fuel tank is varied. The classical mechanic's method cannot analyze and answer the fuel tank of various schemes at the same time, and there can be no measured data at the beginning of the design. Therefore, it is significant to check the strength and stiffness of the fuel tank effectively and quickly and find out the weak links of the fuel tank to provide a reference for the design and modification of the automobile fuel tank. At the same time, to shorten the development cycle, improve the quality of development, adapt to the rapid growth of the market requirements, and enhance the competitiveness of the product market have important practical significance. However, the fuel tank manufacturer still stays at the stage of trial and error in the design of fuel tank structure, mainly relying on the experience of designers, and hardly calculates and optimizes the shape of reinforcing ribs, the thickness of the tank wall, the aperture of the wave-proof plate, and so on, which results in the unreasonable distribution of the material of the tank. The general design process is to manually make fuel tank product samples at first and then to find out the problems by testing and modifying them. From design to the factory, a product needs a long design cycle. Particularly for the fuel tank, it has a large volume, complex structure, and many related inspection indicators, which leads to an increase in production costs.

The fuel tank impact test is a simulated impact test of the product. The purpose of this test is to verify the product is qualified in all aspects of the product when it is subjected to external force shock or external force under normal operating conditions.

Because collision action is a complex process, it is affected by many factors, such as the constraints of the collision body, the relative speed of contact, the geometry and duration of the contact surface, local plastic deformation, and so on [1–3]. Aiming at the collision model of the system, Stronge et al. analyzed the energy change during the oblique collision and the velocity relationship before and after the collision and established the dynamic model of viscous/sliding friction contact [4]. The CEL method is used to simulate the dynamic response of liquid storage vessel in the process of drop collision and the space motion state of liquid

at different times. By comparing with the results of previous literature, the dynamic response and space state in the process of drop collision are discussed in four cases, namely, different drop angle, drop height, vessel thickness, and liquid storage capacity, and the impact of factors on the vessel is also discussed [5]. The composite structure is vulnerable to all kinds of low-energy impact during the process of production and application, which will make invisible visual damage in the laminates and degenerate the mechanical properties of the composite. Composite laminate is closely related to structural safety and life expectancy. So, it is significant to evaluate the low-energy impact resistance and damage prediction of composite structures.

In a variety of collision detection algorithms, the oriented bounding box algorithm had widely used. By using the characteristics of the triangle surrounded by the rectangle in the leaf node and the value calculated in the rectangle-rectangle intersection test phase, the new algorithm contains a better triangle-triangle intersection algorithm in the oriented bounding box. The two triangles are converted into the same coordinate system and then test the two triangles., but this step could be omitted by using the coordinates of the bounding boxes to replace the coordinates of the triangles. This method reduces a lot of redundant coordinate transformation operations compared to the original algorithm [6]. Chai and Wu established a single-degree-of-freedom collision vibration model and studied the effects of parameters, such as collision clearance, damping, stiffness, and excitation frequency, on the bifurcation and chaos phenomena of the system motion using nonlinear dynamic analysis and numerical simulation [7]. Fan et al. use the penalty stiffness method in the contact algorithm, by adjusting the penalty stiffness value reasonably, controlling the penetration distance effectively, and avoiding the ill-conditioned stiffness matrix, which makes the calculation result approach the true value [8]. Collision detection is a hot topic in computer graphics, augmented reality, human-computer interaction, and other fields. In recent years, real-time simulation of large-scale complex scenes has attracted many scholars' attention, especially the emergence of cloud computing and big data technology, which puts forward higher requirements for real-time scene simulation, which also brings unprecedented opportunities and challenges to researchers. As the geometric complexity of the virtual environment increases, the computational complexity of collision detection greatly improved, and the interaction of complex scenes consumes a lot of computer resources. Therefore, the fast collision detection problem has become a bottleneck in the virtual environment. How to design an efficient collision detection algorithm to meet the requirements of real time and accuracy has become a current problem to be solved. Qu had put forward a multiple date parallel collision algorithm based on optimization operator. The search space is confined in a nonuniform local minimum area to reduce the colony search time [9]. Chen et al., based on the local search algorithm of surface, characterized the contact sheet by the coordinates of the center of the face and the length of the feature, carried out presearch to quickly eliminate potential contact pairs that would not occur contact, eliminated the blind area of contact search, and had good robustness and calculation accuracy [10]. Li et al. propose an improved collision detection algorithm based on deformable objects, which is difficult to solve the real-time and fidelity problems of deformable objects. To improve the efficiency of collision detection, an improved particle selection method and the idea of a multiswarm particle optimization algorithm are used to construct a multiline group on the multiline composed of the control point cluster and the center point of the Snake model [11]. Due to the short action time of external transient load and the difficulty of experiment control, the measured data are limited, and the continuous results in space and time are not obtained. Wang simulated and analyzed the drop of metal cylinder structure under empty shell condition by ANSYS/LS-DYNA software and studied the strain distribution law of metal thin-walled cylinder structure under different drop conditions (different height and different fall angle). The variation of stress and impact duration, impact force, and peak overload (impact acceleration) are discussed [12]. An algorithm for simulating friction contact between soil and rigid or flexible structure in the SPH frame is proposed [13]. The calculation domain divides into several subdomains, and the contact force is used as a bridge to establish the connection between the subdomains to finally realize the global solution. When the SPH discretizes governing equations of soil motion in each subdomain, the inherent boundary defects of SPH are corrected. It makes the SPH particles near the contact boundary have accurate acceleration, which ensures the accuracy of contact detection. It is assumed that the soil SPH particles are allowed to invade the structure locally. According to the allowable residual invasion amount and the principle of momentum, normal and tangential contact forces of the contact surface are corrected by the slip condition so that they do not exceed the limit friction. Compared with the existing methods that usually use "particle-particle" contact or ignore friction slip in SPH, the method has higher calculation efficiency and accuracy. It is suitable for the simulation of the interaction between geotechnical materials and rigid or deformable structures. The accuracy and stability of this method verifies in many examples. The calculation shows that the SPH is based on a contact algorithm. The results are in good agreement with the theoretical solution or the finite element solution. The algorithm is effective and can be used to expand the calculation ability and application scope of the SPH. Considering the fluid-structure interaction effects in the analysis of liquid storage container dropping [14], CEL method simulates the inertia effect of fluid and the lateral hydraulic pressure to the container, and the fluid-structure interaction effects on the deformation and dynamic response of the container during the process of dropping are considered. The numerical result shows that the method can provide a more accurate evaluation of vessel safety and structural design. Therefore, the CEL mentioned in the paper also provides a reference design evaluation method for the same structure. Considering particularity and uncertainty of drop impact crashworthiness design, the dynamic response of drop impact and impact crashworthiness robust design has been made. Drop

impact crashworthiness robust design optimize is based on crashworthiness evaluation for virtual drop test [15]. This work enriches the design theory and method for dynamic design. Precision electronic products mobile hard disk and liquid-solid coupled fluid-filled containers are chosen as two samples to investigate the capability of dynamic drop impact, crashworthiness design, optimism of structural parameters, and design of crashworthiness.

The collision of the fuel tank is a transient energy conversion process in which the material absorbs energy through deformation. However, the structure of the fuel tank is sophisticated, which will lead to long calculation time and difficulty to ensure accuracy in collision operation. Aimed at the structural characteristics of the fuel tank, this paper adopts a defense node algorithm that avoids solving simultaneous equations and ensures constraints and accurately calculates contact force.

2. Kinetic Analysis of Tank Collision

2.1. Collision Mechanical of Materials. For the collision body made of the fuel tank, the maximum shear stress σ_τ is related to the surface pressure. The following simple formula expresses their relationship [16].

$$\sigma_\tau = \left[(1+v)\left(s\cot^{-1}s^{-1}\right) + \frac{3}{2\left(1+s^2\right)}\right]q_0(t). \tag{1}$$

Among them, v is the velocity at contact.

The maximum value of σ_τ occurs at $s \approx 2/(1+v)\pi$ and $q_0(t)$ is the maximum surface pressure at given time t. For materials with low shear strength, collision will cause shear failure near the surface. The maximum value occurs at $0.5\,t_0$, and then its duration occurs at t_0. The equivalent plastic strain criterion is used for the failure of fuel tank structural materials. When the equivalent plastic strain of the element reaches the threshold, the material is destroyed, and the corresponding part is deleted.

2.2. Fluid-Solid Coupling Analysis. The dynamic characteristics of liquids are affected by the geometrial parameter, filling height, internal structure distribution, frequency, and amplitude of load excitation. At the same time, the physical properties of liquids, such as density, compressibility, and viscosity, also have different effects on the dynamic performance.

The basic principle of the continuum equation is the conservation of mass. The mass δm contained in the Lagrangian infinitesimal fluid unit $\delta V$is as follows [17]:

$$\delta V = \rho \delta m. \tag{2}$$

In the formula, m is mass and ρ is density.

For the mass conservation is satisfied in the Lagrangian fluid unit, the mass does not change with time; that is to say, the following equation is satisfied.

$$\frac{\mathrm{d}\delta m}{\mathrm{d}t} = \delta V\frac{\mathrm{d}\rho}{\mathrm{d}t} + \rho\frac{\mathrm{d}\delta V}{\mathrm{d}t}. \tag{3}$$

The fluid is a uniform, nonviscous, and incompressible theoretical fluid, ignoring the fluid-solid momentum transfer and the local pressure-density linear relationship [18]. The coupling equation is

$$\begin{bmatrix} M_s & 0 \\ A^T & M_f \end{bmatrix}\{\ddot{u}\ \ddot{p}\} + \begin{bmatrix} K_s & -A \\ A^T & K_f \end{bmatrix}\begin{Bmatrix} u \\ p \end{Bmatrix} = \begin{Bmatrix} F_s \\ F_f \end{Bmatrix}. \tag{4}$$

Here, M_s and K_s are the mass matrix and stiffness matrix of the structure; M_f and K_f are the mass matrix and stiffness matrix of the fluid, respectively; A is a fluid-solid coupling matrix; F_s and F_f are structural loads and acoustic loads, respectively; u is the structural node displacement vector; and p is the fluid node pressure vector.

On the coupling interface Γ, the displacement and load balance conditions meet the following formula:

$$\begin{aligned} d^s \cdot e^s + d^f \cdot e^f &= 0, \\ \sigma^s \cdot e^s + \sigma^f \cdot e^f &= 0. \end{aligned} \tag{5}$$

Here, d^s and d^f are the displacement vectors of the solid domain and fluid domain interfaces, respectively. σ^s and σ^f are the stress vectors at the interface of the solid domain and the fluid domain, respectively. e^s and e^f are the unit displacement base vectors of the solid domain and the fluid domain interface, respectively.

3. Contact Analysis

3.1. Research on Contact Problems during Collision Contact. The collision process of the fuel tank has nonlinear characteristics. When the collision height is short and the impact energy is small, the elastic force $F(x)$ of the cushioning material has a linear relationship with the deformation x. That is to say, simplifying the buffer material becomes a single-degree-of-freedom spring-mass system with a constant stiffness coefficient in the process of drop impact.

The dynamic impact process is a series of dynamic processes varying with time. Subjected to shock excitation, the system will produce a corresponding shock response. It proves theoretically that the maximum value is related to the duration of shock τ and the inherent period T_n of the system itself after shock excitation. When $T_n < \tau$, the maximum shock response of the system may be twice the peak value of the shock wave, while when $T_n > \tau$, the shock response will be weakened. The impact process is a transient energy conversion process, and the buffer material absorbs energy through deformation.

3.1.1. Kinematic Constraints. The contact and collision structure of the fuel tank is shown in Figure 1. When two contacts are in contact, two points x_2^t and x_1^t coincide at the contact interface. Point x_2^t is the orthogonal projection of point x_1^t on boundary Γ^1 of contact 1 on boundary Γ^2. According to kinematic constraints, the formula is as follows [19].

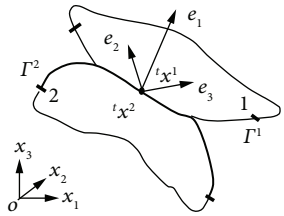

Figure 1: Contact-impact interface model.

$$\left(x_1^t - x_2^t\right) \bullet e_1 \geq 0. \tag{6}$$

Among them, e_1 is the usual unit vector.

3.1.2. Dynamic Constraints. The contact force on the unit contact surface is pressure, and its pressure value p_e should be satisfied.

$$p_e > 0. \tag{7}$$

The tangential friction p_{et} on the contact surface is the resultant force of the tangential contact forces in the other two directions.

$$p_{et} = \sqrt{p_{et2}^2 + p_{et3}^2}. \tag{8}$$

Among them, p_{et2} and p_{et3} are the tangential friction forces of unit tangent vectors e_2 and e_3, respectively.

If the Coulomb friction model is adopted, when the maximum static friction force is less than the maximum static friction force, the points on the two contact surfaces are relatively static; that is, the relative tangential velocity A of the points on the two contact faces is

$$v_t^t = \left(v_1^t - v_2^t\right) - \left[\left(v_1^t - v_2^t\right) \cdot e_1\right] e_1 = 0. \tag{9}$$

Among them, v_1^t and v_2^t are the tangential relative speeds of points x_1^t and x_2^t, respectively.

When it is equal to the sliding friction, point x_1^t and point x_2^t are relatively slipped:

$$v_t^t \bullet \left[p_{1,c}^t - p_{1,c}^t \cdot e_1\right] e_1 \leq 0. \tag{10}$$

Because the collision time is short and the tangential force is relatively small relative to the normal force, the influence of the tangential force during the collision is ignored.

3.2. Contact Force Algorithm for Contact Collision. Through the analysis of the contact interface, the contact point is found out, and then the contact force is calculated by using the motion law of the object. The value of the contact force contact constraints is limited. The contact point is not allowed to penetrate the contact boundary, and the contact force cannot be tensile.

The usual methods to calculate the contact force are the penalty function method and the Lagrange multiplier method. These two methods are quite different in the explicit algorithms and the implicit algorithms. Lagrange multiplier method involves solving the simultaneous equations of unknown contact forces, which cannot be directly used in the explicit algorithm; in contrast, it does not solve any simultaneous equations. Therefore, in the explicit algorithm, the penalty function method is often used to calculate the contact force.

The penalty function method has the disadvantages of introducing artificial error and affecting the stability of the explicit algorithm. To make the error introduced by penalty function method small enough, choose reasonable penalty parameters, effectively control the stability of it, and select appropriate penalty parameters is the most significant problem of using penalty function method to calculate contact force. Another one is the calculation of contact penetration. To avoid the error caused by the penalty function method and the influence on the stability of the solution, some particular algorithms are used to solve the contact force by the Lagrange multiplier method, which avoid solution of the simultaneous equations.

For implicit algorithm, whether the penalty function method or Lagrange multiplier method is used, it involves the establishment of contact stiffness matrix, and different iterative algorithms have different requirements for contact stiffness matrix. In the implicit algorithm, a new contact point may not only affect the number of zero elements in the coefficient matrix of the algebraic equation but also affect the bandwidth of the coefficient matrix. When using the Lagrange multiplier method, the total number of unknowns increases, which leads to the change of dimension of the coefficient matrix. So, these will affect the memory allocation and management in the process of solving and also affect the calculation workload. In the implicit algorithm, if the penalty function method is used to calculate the contact force, the penalty parameter should not be too large; otherwise, the coefficient matrix may become ill-conditioned and hinder the solution.

The contact algorithm accomplishes the interaction between colliding structures or components. Within each time step of the solution, check whether the slave node penetrates the main surface. If it penetrates, the force is applied in a direction perpendicular to the main surface by a penalty function to prevent further penetration of the slave node, if not worn. Pass through and then proceed. In the penalty function method, it is difficult to select the penalty parameter value, and it is difficult to obtain the ideal calculation result by experience. To ensure accuracy, the defense node method is used to calculate the contact force. That is, the Lagrange multiplier method is used to satisfy the constraints accurately, and the algorithm of solving simultaneous equations is avoided. The defense node is calculated by adding a virtual contact point to each contact pair.

Assuming the mass of the defense node is M, the motion equation of the defense node and the contact point can be written as follows [20].

$$\begin{aligned} M_1 a_1 &= F_1 + f_1, \\ M_2 a_2 &= F_2 + f_2. \end{aligned} \tag{11}$$

Among them, subscripts 1 and 2 represent, respectively, from the contact point and the defense node. F and f are normal force and contact force, respectively.

The Lagrange multiplier method is used to calculate the contact force to satisfy the constraints. The motion equation is obtained by using the central difference method from the contact point and the defense node.

$$M_1\frac{\left[{}^{\tau}v_1-\left({}^{t}s_1-{}^{\tau}s_1\right)/\Delta t\right]}{\Delta t}={}^{\tau}F_1+{}^{\tau}f_1,$$
$$M_2\frac{\left[{}^{\tau}v_2-\left({}^{t}s_2-{}^{\tau}s_2\right)/\Delta t\right]}{\Delta t}={}^{\tau}F_2+{}^{\tau}f_2. \tag{12}$$

Among them, ${}^{\tau}s$, ${}^{\tau}v$ are the displacement and velocity after contact; ${}^{\tau}s$, ${}^{\tau}v$ are the displacement and velocity before contact.

According to the same magnitude of the defense point force and the force from the contact point, the normal distance is 0, and the defense node force is 0.

$${}^{\tau}f_1=M_1M_2\frac{\left({}^{\tau}F_2/M_2-{}^{\tau}F_1/M_1+{}^{l}v_2/\Delta t-{}^{l}v_1/\Delta t-{}^{\tau}g/\Delta t\right)}{\left(M_1+M_2\right)}. \tag{13}$$

Among them, ${}^{\tau}g$ is the total gap between the defensive point and the contact point.

The contact search algorithm plays a significant role in reducing calculation time and improving calculation accuracy. Any contact level has its contact domain, which can be defined as an extension domain. If a slave falls into an extension domain of the main block, the two may contact to form a test pair. If a slave falls into the contact area of it (edge, point), the two contact and shape a contact pair [21].

Contact search includes precontact search and postcontact search. The precontact search is usually divided into two steps, namely, global search and local search, for the slave points that are not in contact state in the previous calculation. The global search roughly determines the slave points that may be contacted and the main blocks that may be contacted with the slave points processed, which is to find out all the test pairs. Local search accurately locates the target of the slave point, calculates the penetration of the slave point relative to its target point, and judges the contact state of the slave point, to find out all contact pairs from the test pair.

Through the contact search algorithm, all the slave points in contact state and their corresponding main blocks (edges, points) in the mechanical system are determined, and the homologous contact force algorithm is used to calculate the contact force. Use the explicit calculation of the central differential and use the contact algorithm to solve the problem. Then, the acceleration of the nodes is used to calculate other physical quantities.

3.3. Stress Failure Criteria. The surface pressure is caused by collision, the failure form is caused by three-dimensional internal stress, and the time sequence of various failure forms. Therefore, appropriate failure criteria can be adopted for the three-dimensional stress state caused by a collision at each point in the collision object. For composite materials, there are three common criteria:

Cai-Hill Tsai-Hill Strength Theory

$$\frac{\sigma_L^2}{F_L^2}-\frac{\sigma_L\sigma_T}{F_L^2}+\frac{\sigma_T^2}{F_T^2}+\frac{\tau_{LT}^2}{F_{LT}^2}=1. \tag{14}$$

Hoffman Failure Criterion

$$\frac{\sigma_L^2-\sigma_L\sigma_T}{F_{Lt}F_{Lc}}+\frac{\sigma_L^2}{F_L^2}-\frac{F_{Lc}-F_{Lt}}{F_{Lt}F_{Lc}}\sigma_L+\frac{F_{Tc}-F_{Tt}}{F_TF_{Tt}}\sigma_T+\frac{\tau_{LT}^2}{F_{LT}^2}=1. \tag{15}$$

Tsai-Wu Tensor Theory

$$\frac{\sigma_1^2}{F_{Lt}F_{Lc}}-\frac{\sigma_1\sigma_2}{\sqrt{F_{Lt}F_{Lc}F_TF_{Tt}}}+\frac{\sigma_2^2}{F_{Lt}F_{Lc}}+\frac{\sigma_6^2}{\tau^2}+\frac{F_{Lc}-F_{Lt}}{F_{Lt}F_{Lc}}\sigma_1+\frac{F_{Tc}-F_{Tt}}{F_TF_{Tt}}\sigma_2=1. \tag{16}$$

For the plane stress-strain state, the improved maximum stress failure criterion is used to judge the failure of the matrix material.

3.4. Analysis of Simulation Results. The fuel tank used in this calculation is shown in Figure 2. According to the requirements of the enterprise, use 348 kg slider impact the fuel tank at the height of 2.04 m, and the fuel tank is filled with liquid. For the convenience of analysis, it is considered that the baffle and the slider are rigid parts, and two points of their collision are taken as test data, respectively. The stress simulation results are shown in the figure.

After the tank collides, the displacement deformation in different directions can be obtained. Since the collision mainly occurs in a different direction, the major deformation is shown in Figure 3.

(a) Before the collision

(b) Displacement diagram in the x-direction after the collision

(c) Displacement diagram in the y-direction after the collision

(d) Displacement diagram in the z-direction after the collision

In terms of displacement, the front end with relatively large deformation is taken. As the fuel tank is a curved part, it is convenient to fix the sensor. The sensor is placed on the plane of the fuel tank in the front section. After measuring its position, the collision and simulation experiments are carried out (Figure 4). In the process of impact test, the major deformation is in the x-axis direction, so this test also mainly considers the impact on the x-axis, and the simulation results are consistent with the experimental results, meeting our impact requirements.

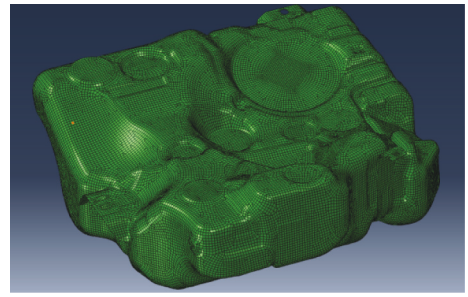

Figure 2: Fuel tank structure diagram.

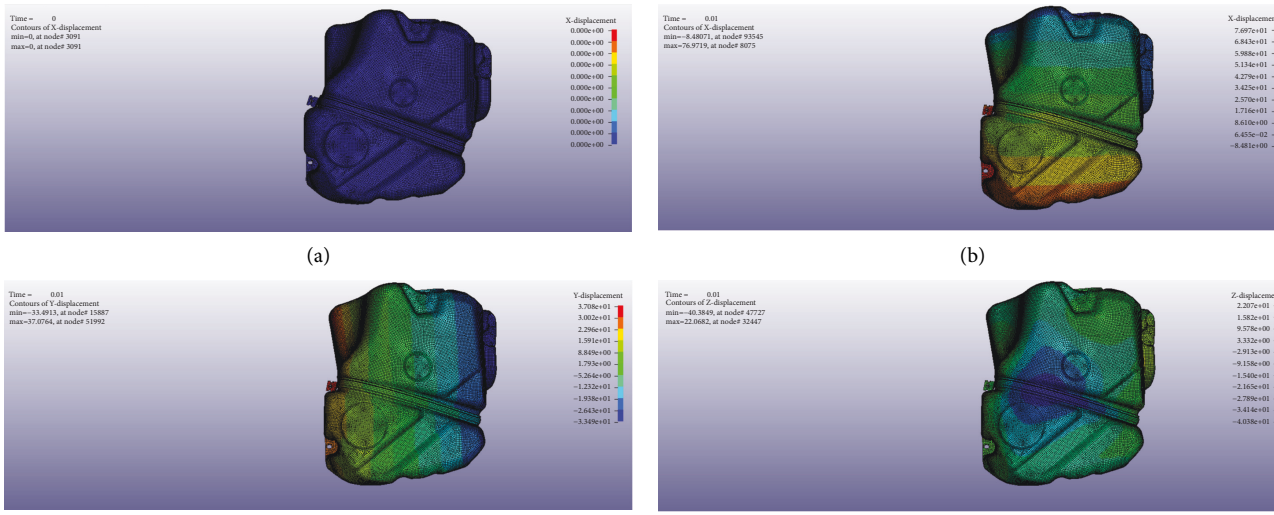

Figure 3: Displacement diagram of the fuel tank. (a) Before the collision. (b) Displacement diagram in the x-direction after the collision. (c) Displacement diagram in the y-direction after the collision. (d) Displacement diagram in the z-direction after the collision.

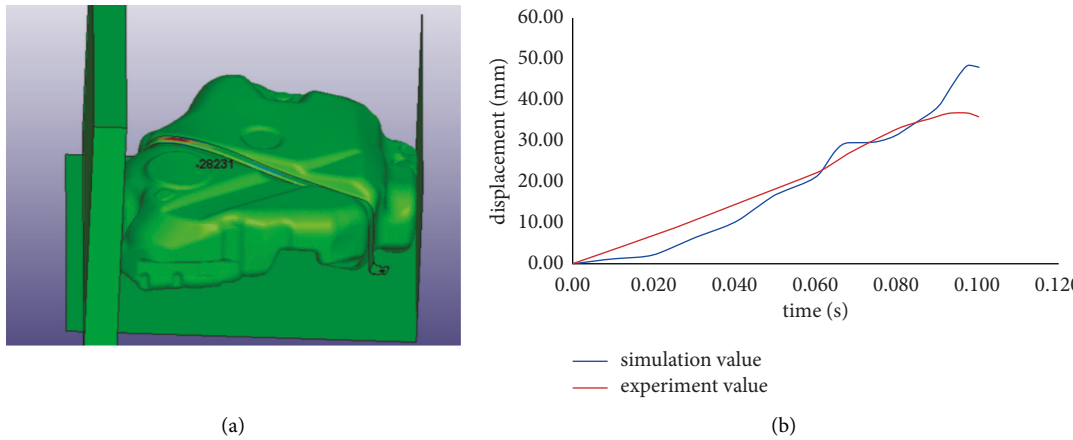

Figure 4: Fuel tank configuration and stress-strain diagram. (a) Test point. (b) X displacement of test point.

4. Conclusion

In this paper, the structure of the fuel tank is analyzed, and the mechanical analysis of the collision body made of the fuel tank is carried out. In the collision operation, the problems such as long calculation time and difficulty to guarantee accuracy are caused. The collision impact process of the fuel tank is analyzed, and the deformation process of the fuel tank is simulated and analyzed by the defense node algorithm. This study has important practical significance for the actual collision process of the fuel tank.

Data Availability

The data that support the findings of this study are available from the corresponding author upon reasonable request.

Conflicts of Interest

The authors declare that there are no conflicts of interest regarding the publication of this paper. The paper was presented as a preprint in Research Square (https://assets.researchsquare.com/files/rs-71519/v1_stamped.pdf).

Authors' Contributions

Wenguang Liu analyzed and supervised the study. Haijiang Liu analyzed the study. Lin Jiang analyzed the study. Shanshan Bi analyzed the study.

Acknowledgments

This work was supported in part by a grant from the Jiangsu Provincial Six Talent Projects Funding (JXQC-009).

References

[1] Y. Gao, Z. Ge, W. Zhai, and S. Tan, "The finite element modelling and dynamic characteristics analysis about one kind of armoured vehicles' fuel tanks," *Materials Science & Engineering Conference Series*, vol. 301, 2018.

[2] S. J. Magdum, A. Das, V. Shetty, R. Sivakumar, and G. Sakthivel, "DOE study of 'the effect of various parameters on fuel tank sloshing using multiphase CFD'," *International Journal of Ambient Energy*, vol. 42, pp. 1–10, 2018.

[3] M. Martin, M. Zmindak, and P. Pastorek, "Dynamic analysis of fuel tank," *Procedia Engineering*, vol. 136, pp. 45–49, 2016.

[4] W. J. Stronge, R. James, and B. Ravani, "Oblique impact with friction and tangential compliance," *Philosophical Transactions of the Royal Society of London,Series A: Mathematical, Physical and Engineering Sciences*, vol. 359, no. 1789, pp. 2447–2465, 2001.

[5] L. H. Zhang, *Finite Element Simulation on Dropping Impact of Liquid Storage Container*, Dalian University of Technology, Liaoning, China, 2014.

[6] C. Liu, X. Jiang, and H. Shi, "Mended collision detection algorithm based on oriented bounding box," *Computer Technology and Development*, vol. 28, no. 6, pp. 49–54, 2018.

[7] L. Chai and X.-M. Wu, "Evolution of bifurcation and chaos in mechanical vibro-impact system with parameters," *Journal of Xiamen University*, vol. 53, no. 4, pp. 508–513, 2014.

[8] J. Fan, M. Wu, and J. Hu, "Dynamic analysis of vehicle-bride interaction based on interfacial contact algorithm," *China Journal of Highway and Transport*, vol. 30, no. 4, pp. 52–58, 2017.

[9] H. Qu, W. Zhao, and A. Qin, "A fast collision detection algorithm based on optimization operator," *Journal of Jilin University (Engineering and Technology Edition)*, vol. 47, no. 5, pp. 1598–1603, 2017.

[10] C. Chen, M. Liu, and X. Chen, "A contact-impact algorithm based on the segment-to-segment local searching method," *Chinese Journal of Computational Mechanics*, no. 1, pp. 105–110, 2018.

[11] Z. Li, Y. Jin, and Z. Qin, "Collision detection algorithm of deformable object-based on Snake model optimization," *Journal of System Simulation*, no. 1, pp. 62–68, 2018.

[12] B. Wang, *Metal Thin-Walled Tube Structure Drop experiment and Simulation*, Beijing Institute of Technology, Beijing, China, 2015.

[13] J. Wang, H. Wu, and C. Gu, "Simulation of friction contact in smooth particle hydrodynamics (SPH)," *China Science: Technology Science*, vol. 56, no. 11, pp. 1208–1218, 2013.

[14] J. Nie, H. Zhang, and H. Li, "Dropping accident analysis of liquid storage container using finite element method," *Nuclear Power Engineering*, vol. 34, no. 3, pp. 145–147, 2013.

[15] S. Yang, *Drop Impact Dynamics and Crashworthiness Robust Design for Manufactured Products*, China University of Mining and technology, Haidian, China, 2009.

[16] Z. Zhang, *A Study on Impact of Composite Material CNG cylinder*, North China University Technology, Beijing, China, 2006.

[17] L. Fu, *Dynamic Analysis of Liquid Sloshing and Sloshing Suppression Design for a Tank*, Nanjing University of Aeronautics and Astronautics, Nanjing, China, 2010.

[18] G. Fu, J. Liang, and H. Luo, "Fluid-structure coupling modal analysis of auto oiltank," *Automotive Technology*, no. 2, pp. 25–28, 2016.

[19] Z. Yang, Z. Zhong, and G. Li, "Review on contact algorithms calculating the contact-impact interface in mechanical system with explicit FEM," *Journal of Mechanical Engineering*, vol. 47, no. 13, pp. 44–58, 2011.

[20] H. Hong and G. Li, "Analysis of sheet metal forming based on defence node algorithm," *Computer Simulation*, vol. 28, no. 8, pp. 320–322, 2011.

[21] W. Liu, H. Liu, L. Jiang, and S. Bi, *Analysis of Fuel Tank Collision Structure Based on Defense point Method*, 2020.